

Unraveling the Interplay between Stability and Flexibility in the Design of Polyethylene Terephthalate (PET) Hydrolases

Shiqinrui Xu, Chengze Huo, and Xiakun Chu*

Cite This: *J. Chem. Inf. Model.* 2024, 64, 7576–7589

Read Online

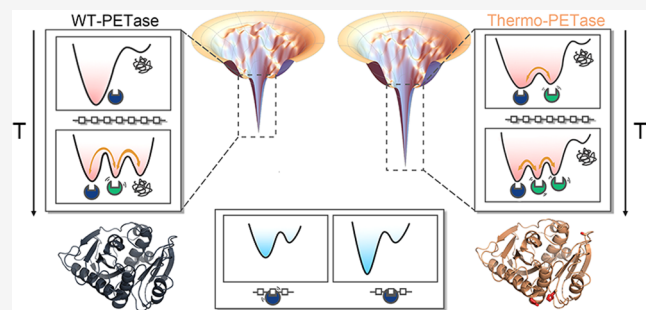
ACCESS |

Metrics & More

Article Recommendations

Supporting Information

ABSTRACT: The accumulation of polyethylene terephthalate (PET), a widely used polyester plastic in packaging and textiles, has led to a global environmental crisis. Biodegradation presents a promising strategy for PET recycling, with PET hydrolases (PETase) undertaking the task at the molecular level. Unfortunately, PETase operates only at ambient temperatures with low efficiency, limiting its industrial application. Current engineering efforts focus on enhancing the thermostability of PETase, but increased stability can reduce the structural dynamics needed for substrate binding, potentially slowing enzymatic activity. To elucidate the balance between stability and flexibility in optimizing PETase catalytic activity, we performed theoretical investigations on both wild-type PETase (WT-PETase) and a thermophilic variant (Thermo-PETase) using molecular dynamics simulations and frustration analysis. Despite being initially designed to stabilize the native structure of the enzyme, our findings reveal that Thermo-PETase exhibits an unprecedented increase in structural flexibility at the PET-binding and catalytic sites, beneficial for substrate recruitment and product release, compared to WT-PETase. Upon PET binding, we observed that the structural dynamics of Thermo-PETase is largely quenched, favoring the proximity between the catalytic residues and the carbonyl of the PET substrate. This may potentially contribute to a higher probability of a catalytic reaction occurring in Thermo-PETase compared to WT-PETase. We suggest that Thermo-PETase can exhibit higher PET-degradation performance than WT-PETase across a broad temperature range by leveraging stability and flexibility at high and low temperatures, respectively. Our findings provide valuable insights into how PETase optimizes its enzymatic performance by balancing stability and flexibility, which may contribute to future PETase design strategies.



INTRODUCTION

Plastics play a vital role in all aspects of everyday life, offering numerous benefits for the development of modern society. However, due to the ultralong lifetimes of most synthetic plastics, plastic waste accumulation has now become one of the most globally challenging environmental crises, profoundly impacting the ecosystems and posing great health risks to both wildlife and humans.^{1–3} Among the various types of plastics, polyethylene terephthalate (PET) is the most abundant thermoplastic polyester manufactured in the world, primarily because of its widespread usage in the packaging market and the textile industry.^{4,5} Despite its prevalence, PET exhibits high resistance to degradation, leading to the accumulation of PET plastic waste after use and contributing significantly to the solid waste problem worldwide.^{6,7}

Great efforts have been made toward PET biodegradation, which is an environmentally friendly and efficient technology, ideal for the closed-loop recycling of PET plastics.⁸ Enzymes that exhibit PET-degradation activity are known as PET hydrolases, and they are capable of breaking down the long-chain PET molecules into their building blocks.^{9–11} Over recent decades, several PET hydrolases have been identified

and studied, including cutinases, lipases, and esterases.^{12,13} Among these, PET-degrading cutinases from thermophilic micro-organisms have shown remarkable PET-degradation efficiency at high temperatures, near the glass transition temperature of PET, where the PET crystalline structure starts to melt toward the amorphous polymer chains.^{13–17} In 2016, Yoshida et al. made a breakthrough discovery of a cutinase-like PET hydrolase, named PETase, in the bacterium *Ideonella sakaiensis*, which can degrade and assimilate PET as its source of carbon and energy.¹⁸ PETase is a naturally evolved PET hydrolase exhibiting high PET depolymerization activity at ambient temperatures. Consequently, this unique property of PETase has distinguished it from PET-degrading cutinases.¹¹ However, PETase showed very low degradation efficiency for

Received: May 20, 2024

Revised: July 22, 2024

Accepted: September 4, 2024

Published: September 13, 2024



highly crystallized PET and rapidly lost its enzymatic activity with increasing temperature.¹⁹ These features impede the practical applications of PETase in the plastics degradation industry.

To increase the thermostability of PETase and further improve the PET-degradation performance, various engineering strategies have been devised.^{20–31} Son et al. discovered that PETase with only three-residue substitution (S121E/D186H/R280A) remarkably enhanced the PET depolymerization activity across different temperatures, compared to wild-type PETase (WT-PETase).²¹ This new variant, named Thermo-PETase, derived from a structure-based protein engineering strategy, was primarily designed to stabilize the flexible loop, which exhibited high B-factor values in the crystal structure. The mutations proposed for Thermo-PETase established the newly formed interactions in the native structure of PETase, thus increasing the melting temperature by 8.8 K compared to WT-PETase.²¹ Similar strategies focusing on mutations of residues to stabilize the most flexible loop in PETase, have been recently developed to successfully achieve increased thermostability.^{32,33} Moving forward, a deep learning method was employed to introduce two additional mutations to Thermo-PETase, giving rise to FAST-PETase.²⁵ FAST-PETase, which demonstrated much higher PET-degradation activity than many other PETase variants, exhibited an increase in melting temperature by 9 K over its scaffold Thermo-PETase. Structural analysis reveals that the increased thermostability of FAST-PETase can be largely attributed to the formation of favorable salt bridges and hydrogen bonds in the native structure. Recently, directed evolution methods have been applied to PETase design, resulting in successful variants capable of operating at the glass transition temperature of PET, presenting a significant step toward complete PET depolymerization.^{26,29}

Despite significant achievements made in the discovery of highly thermostable PETase variants,^{34–36} progress toward finding PETase capable of operating efficiently at ambient temperatures has been proceeding slowly. This is largely due to the fact that our understanding of the structure–function relationship in PETase remains elusive.^{19,37–39} It has been recognized that, unlike other thermophilic cutinases, the unique property of PET-degradation activity at ambient temperatures for PETase is attributed to its open and flexible substrate-binding cleft.⁴⁰ Increasing evidence has revealed that modulating the opening of the binding cleft in thermophilic cutinases can enhance their catalytic efficiency on PET degradation,^{41,42} highlighting the importance of structural flexibility at the substrate-binding site of PET hydrolases in facilitating enzymatic activity. However, by narrowing down the binding cleft on the surface of WT-PETase through mutations, Austin et al. observed increased hydrolytic activity on PET,³⁸ leading to the seemingly conflicting effects of structural dynamics in PETase on exerting its catalytic function. Furthermore, increasing the thermostability of PETase is generally achieved by introducing newly formed interactions to stabilize the native structure.^{43,44} Thus, reducing the structural flexibility in the native state of PETase, a common strategy for improving stability in PETase design, may be disadvantageous to substrate binding and product release, potentially slowing the catalytic activity. Understanding the interplay between stability and flexibility in PETase is fundamental and crucial for further engineering efficient PET

hydrolase operating at ambient temperature, but it presents great challenges.

In this work, we performed molecular dynamics (MD) simulations along with frustration analysis on WT-PETase and one prototypical thermophilic PET variant, Thermo-PETase, which was observed to exhibit an overall enhanced PET hydrolytic activity over WT-PETase across a wide range of temperatures.^{21,25} Consistent with experimental findings, our simulations show that Thermo-PETase unfolds more slowly than WT-PETase at high temperatures,²¹ thus allowing Thermo-PETase to maintain its functional activity for a longer duration at elevated temperatures. Interestingly, despite the increase in global stability led by mutations, we observed that Thermo-PETase possesses more significant structural flexibility than WT-PETase at ambient temperatures. Our detailed analyses unveil that the structural dynamics at the PET-binding site and catalytic triad in Thermo-PETase are more pronounced, potentially facilitating substrate recruitment and product release compared to WT-PETase. Additionally, frustration results indicate that there are large-scale arrangements of frustrated contacts in Thermo-PETase upon mutations, leading to an increased degree of frustration at the local binding site while maintaining global scales unchanged. Moreover, we found that the structural dynamics of Thermo-PETase within the substrate–enzyme complex are largely quenched by the interactions formed with PET, resulting in a stable bound complex state primed for subsequent highly efficient chemical reactions. Our results provide valuable insights into the future rational design of PETase and other PET hydrolases toward PET degradation at ambient temperature by balancing global stability and local flexibility.

MATERIALS AND METHODS

MD Simulations of apo PETase. We performed all-atom MD simulations using Gromacs-2023.2 software⁴⁵ with Amber ff14SB force field.⁴⁶ Simulations were initialized from the native structures for WT- and Thermo-PETase (PDB: 5XJH¹⁹ and 6IJ6²¹), respectively. Given the complex environmental conditions under which PETase may function, all amino acids in the enzyme are modeled at their standard protonated states at pH 7. The native structures of WT- and Thermo-PETase were individually placed in a cubic box with margins of 1.0 nm. The protein systems were then solvated with the TIP3P water model and the salt concentration was set to 100 mM to mimic the *in vivo* environment. For WT-PETase, the box length was 7.50 nm, including 25 NA^+ ions, 30 CL^- ions, 12 385 water molecules, and a total of 40 928 atoms. For Thermo-PETase, the box length was 7.47 nm including 25 NA^+ ions, 31 CL^- ions, 12369 water molecules, and a total of 40 930 atoms. A short energy minimization step was performed for each system using the steepest descent algorithm, with a maximum of 50000 steps and a maximum force threshold of 1000 kJ/mol/nm. After energy minimization, systems were equilibrated in the NVT phase using the V-rescale thermostat for 100 ps, with temperature coupling time constant $\tau_t = 0.1$ ps. Subsequently, the NPT equilibration simulations were conducted using the Parrinello–Rahman barostat for 100 ps with the relaxation time constant $\tau_p = 4.0$ ps and the reference pressure of 1.0 bar.⁴⁷ During MD simulations, the LINCS algorithm was used to constrain all hydrogen bonds,⁴⁸ allowing for a time step of 2 fs. The particle-mesh Ewald (PME) method was employed to compute the long-range electrostatic interactions⁴⁹ and all the

nonbonded interactions were cut off at 1.0 nm. Periodic conditions were applied in all three directions. Temperature coupling was applied separately to protein and nonprotein groups. Isotropic pressure coupling was used to ensure uniform scaling of the box vectors. Production simulations were run in the NPT phase for 10 μ s at the ambient temperatures (298 and 308 K) and for 1 μ s at an elevated temperature of 450 K. For each PETase system, two trajectories were performed at both 298 and 308 K, and five trajectories were performed at 450 K.

Molecular Docking. We constructed the complex structure of PETase with a PET tetramer (4PET) by molecular docking. The initial coordinates of PETase were chosen from the Protein Data Bank (PDB: 5XJH¹⁹). PETase was selected as the receptor in AutoDockTools⁵⁰ and converted to PDBQT format, which is similar to the PDB format but specifically designed to contain the information required by AutoDock software. We used 2-hydroxyethyl-(monohydroxyethyl terephthalate)₄ (2-HE(MHET)₄) as the PET tetramer ligand. The PET tetramer was constructed by combining two PET dimers and carefully adding one ethylene glycol moiety to its terephthalate terminal using Avogadro software.^{51,52} All hydrogen atoms were added to both protein and ligand using AutoDockTools prior to docking.⁵⁰ Molecular docking was carried out between the WT-PETase structure and 2-HE(MHET)₄ using AutoDock Vina (version 1.1.2).⁵³ During docking, the ligand was set to be flexible, while the protein was kept rigid. To prevent the collapse of the PET chain, the three bonds within the O—C—C—O group connecting the second and third benzene rings and the central C—C bond connecting the first and second benzene rings of the PET ligand were constrained from rotating. The top five docking structural models were analyzed to examine hydrogen bonds and π — π interactions between PETase and 4PET. The docking model, which is the most consistent with those from previous studies,^{19,54} was selected and further evaluation of the structure model was done by MD simulations.

MD Simulations of PETase:4PET Binary Complex. MD simulations of the PETase:4PET complex, starting from the docking model were performed using Gromacs-2023.2 software,⁴⁵ following the same protocols as those used for simulations of the apo state of PETase. The PET ligand, consisting of 98 atoms, was parametrized with the general Amber force field (GAFF2)⁵⁵ and the topology files of 4PET for Gromacs simulations were prepared using ACPYPE software.⁵⁶ To model the complex structure of Thermo-PETase with 4PET, we directly introduced three mutations into WT-PETase using PyMOL software.⁵⁷ The simulation box was set to be cubic, with a length of 7.43 nm. The system was solvated with 12 330 and 12 338 TIP3P water molecules for WT- and Thermo-PETase, respectively. To realize the electrostatically neutral environment with the salt concentration of 100 mM, we added 25 NA+ and 31 Cl- ions for the WT-PETase system and 25 NA+ and 30 Cl- ions for the Thermo-PETase system, resulting in a total of 40 938 and 40 956 atoms, respectively. For each PETase system, two trajectories each with a length of 1 μ s were generated at both 298 and 308 K without implementing any restraints on the enzyme and substrate, following previous studies.^{40,51,58,59} We found that 4PET maintained binding interactions with both WT- and Thermo-PETase throughout the 1 μ s MD simulations.

Computational Analysis. We used the built-in modules of Gromacs to calculate root-mean-square deviation (RMSD),

root-mean-square fluctuation (RMSF), residue distances, and to conduct principal component analysis (PCA), while the MDAnalysis software was employed for calculating the contact map.⁶⁰ All of the analyses were performed after the removal of the translation and rotation of the protein in the simulation system during the trajectories. The RMSF value for each residue was calculated by averaging the RMSF of atoms belonging to that residue. For contact probability calculations, contacts between any heavy atoms of one residue pair were included with the cutoff distance set at 0.5 nm. The results were normalized to obtain the residue-level contact probability. The two-dimensional (2D) free energy landscapes (FELs) were constructed using the formula: $-kT \ln P(x, y)$, where $P(x, y)$ is the probability distribution of the protein configuration at the selected reaction coordinates x and y obtained from the simulations. All trajectories at ambient temperatures (298 and 308 K) were combined together for calculating $P(x, y)$.

PCA transforms a number of correlated variables into a number of uncorrelated variables called principal components (PCs), while retaining those characteristics of the data set that contribute most to its variance.⁶¹ The PCA results show the directionality and amplitude of protein motions with the first several PCs correlated with large conformational changes. PCA was performed on the trajectories of 298 and 308 K, respectively. At each temperature, two trajectories were combined together and the Cartesian coordinates of C_{α} atoms of residues were chosen to calculate the covariance matrix C . The elements of covariance matrix C were calculated by

$$C_{ij} = \frac{1}{N} \sum_{k=1}^N (\mathbf{r}_i^k - \langle \mathbf{r}_i \rangle)(\mathbf{r}_j^k - \langle \mathbf{r}_j \rangle)$$

where N is the total number of simulation frames, \mathbf{r}_i^k is the Cartesian coordinate of C_{α} atom of residue i at the simulation frame k and $\langle \mathbf{r}_i \rangle$ denotes the average over the entire trajectory. The eigenvalues and eigenvectors were calculated by diagonalizing covariance matrix C . Each eigenvalue represents the mean displacement along the corresponding eigenvectors. The two eigenvectors associated with the two highest eigenvalues account for the two largest percentages of the total fluctuations, corresponding to PC1 and PC2, respectively. The trajectories were finally projected onto PC1 and PC2 for further analysis.

Frustration results were obtained by using the Frustrometer online server.⁶² The PDB files of WT- and Thermo-PETase (5XJH¹⁹ and 6IJ6²¹) were uploaded to the server with electrostatic interactions considered during the calculation. The frustration index ($FruInd$) measures how favorable a native contact is relative to the set of all possible contacts by mutation of the residues in that location, normalized using the variance of the energy distribution. In practice, we used “configurational frustration” to obtain $FruInd$, as this option takes into account residue changes in both identity and location. A contact is defined as “minimally frustrated” if $FruInd$ is higher than 0.78, indicating that its native energy is at the lower end of the energy distribution. Conversely, a contact is defined as “highly frustrated” if $FruInd$ is lower than -1, indicating that its native energy is at the higher end of the energy distribution.

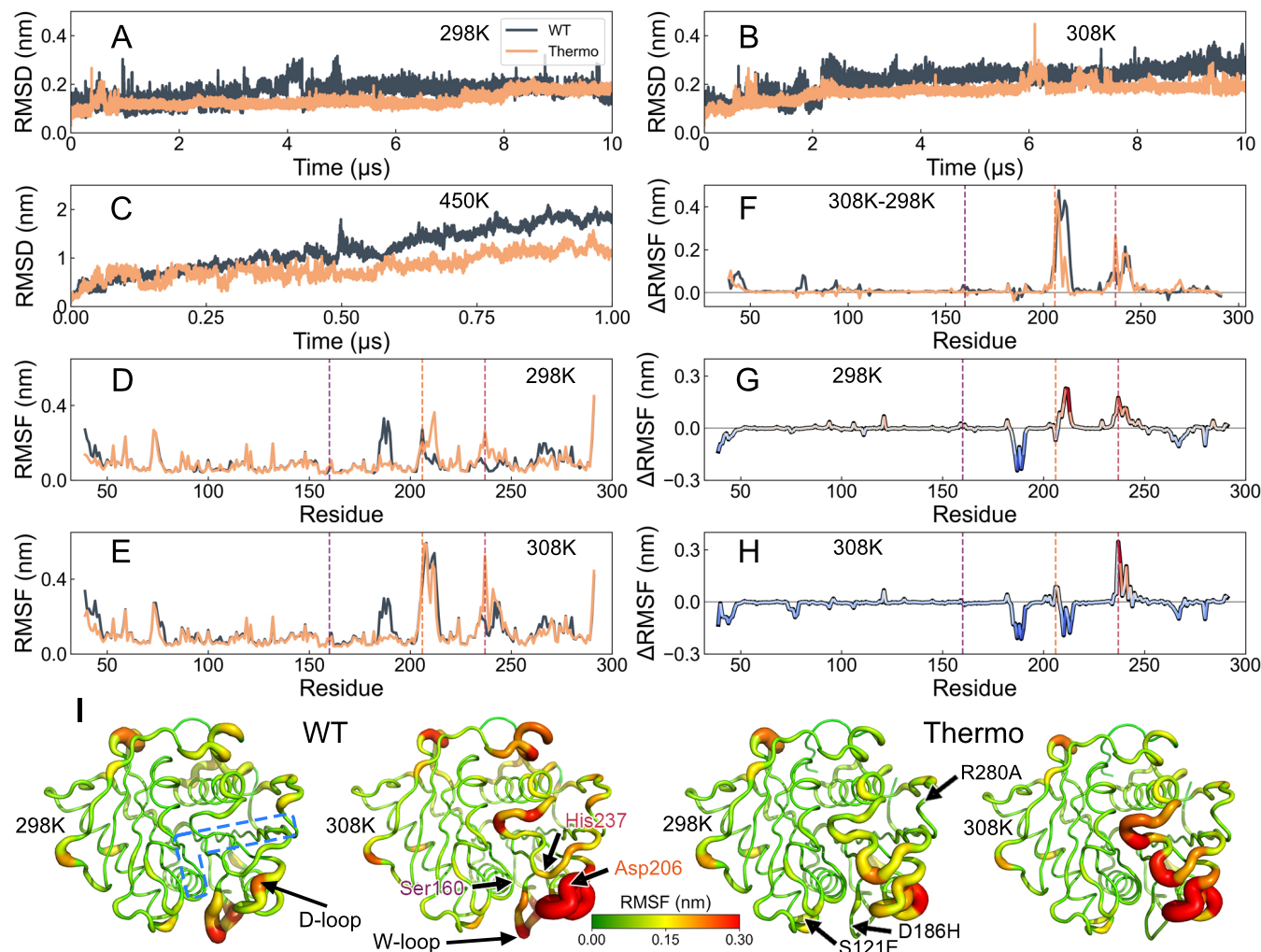


Figure 1. Structural stability and flexibility of WT- and Thermo-PETase revealed by MD simulations. RMSD relative to the corresponding native structures of WT- and Thermo-PETase (PDB: 5XJH¹⁹ and 6IJ6²¹) at (A) 298 K, (B) 308 K, and (C) 450 K, respectively. RMSF of WT- and Thermo-PETase at (D) 298 K and (E) 308 K. (F) RMSF differences between 298 and 308 K for WT- and Thermo-PETase. RMSF differences between WT- and Thermo-PETase ($\text{RMSF}_{\text{Thermo}} - \text{RMSF}_{\text{WT}}$) at (G) 298 K and (H) 308 K. The purple, orange, and red vertical lines in (D–H) indicate the catalytic triad Ser160, Asp206, and His237, respectively. (I) RMSF values at 298 and 308 K for WT- and Thermo-PETase projected onto the corresponding native structures. The thickness and color of the tubes illustrated on the PETase structures denote the magnitudes of RMSF. The blue dashed region in (I) illustrates the PET-binding site on the surface of PETase. The PET-binding site is determined by the docking of one PET tetramer to WT-PETase, as described in Figure S1. The three mutations (S121E/D186H/R280A) in Thermo-PETase with respect to WT-PETase are indicated in (I).²¹

RESULTS AND DISCUSSION

Structural Dynamics of PETase in the Native State.

We performed microsecond-long MD simulations initialized from the native structures of WT- and Thermo-PETase to investigate the temperature-dependent structural dynamics of PETase. MD simulations were carried out at two ambient temperatures (298 and 308 K) and one elevated temperature (450 K), which is much higher than the melting temperatures of WT- and Thermo-PETase measured by experiments (321.8 and 330.6 K).²¹ RMSD relative to the respective native structures was then calculated for each simulation. We observed that Thermo-PETase consistently exhibits lower RMSD values than WT-PETase at all three temperatures, in particular, at the high temperature of 450 K (Figures 1A–C, S2). These results suggest that Thermo-PETase possesses enhanced thermodynamic stability upon the mutations, consistent with experimental observations.²¹ Additionally, the consistently lower RMSD values of Thermo-PETase compared

to WT-PETase at both 298 and 308 K imply an overall reduction in the structural dynamics of Thermo-PETase relative to WT-PETase.

To quantitatively assess the structural dynamics of PETase at the residue level, we calculated RMSF by collecting all the simulation trajectories each at 298 and 308 K (Figure 1D and E). The RMSF profiles and residue-level contact probability maps of WT- and Thermo-PETase show substantial overlap at both corresponding temperatures, with notable differences primarily observed in the region involving Trp185 (within the W-loop, Ala180–Pro197), and the region involving Asp206 (within the D-loop, Glu204–Ser213) and His237 of the catalytic triad (Figure S3). As the temperature increases, the structural flexibility of these two catalytic residues (Asp206 and His237) in both WT- and Thermo-PETase appears to be significantly enhanced (Figure 1F). Interestingly, although the overall structural dynamics of WT-PETase is more significant than those of Thermo-PETase, as indicated by RMSD (Figure

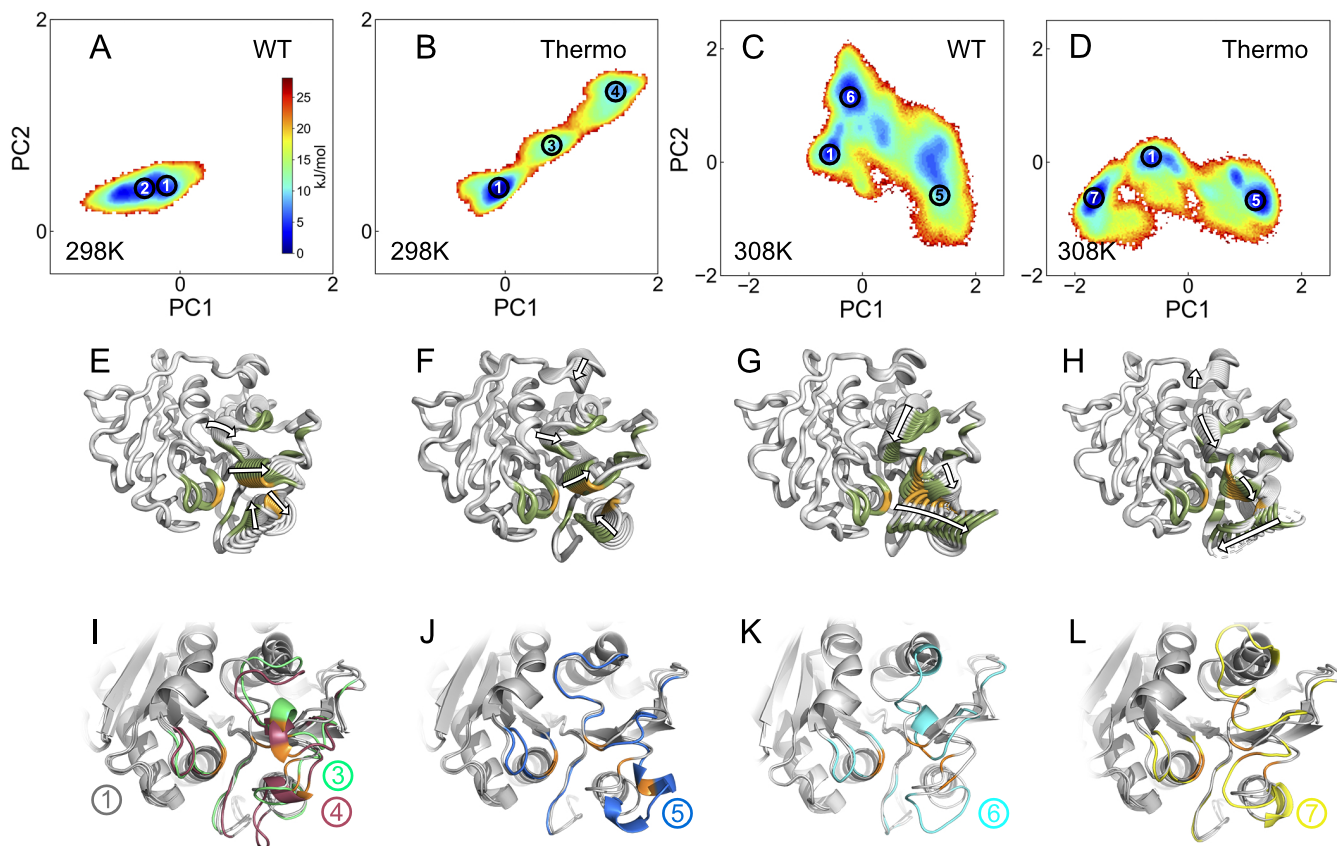


Figure 2. PCA projected on the native dynamics of WT- and Thermo-PETase. (A, B) FELs of WT- and Thermo-PETase at 298 K, projected onto PC1 and PC2. The weights of PC1 and PC2 are 20.89 and 15.35%, respectively. (C, D) FELs of WT- and Thermo-PETase at 308 K, projected onto PC1 and PC2. The weights of PC1 and PC2 are 29.19 and 12.18%, respectively. Representative structures of PETase extracted from the simulation trajectories at 298 K projected onto (E) PC1 and (F) PC2, respectively. Representative structures of PETase extracted from the simulation trajectories at 308 K projected onto (G) PC1 and (H) PC2, respectively. In each panel of panels (E–H), 10 representative structures ranging from the lowest to the highest PC values are shown, with arrows indicating the structural motions along the corresponding PC. (I–L) Local PETase structural illustrations focusing on the PET-binding site for different (meta)stable states indicated in (A–D). The PDB structure of WT-PETase (gray, representing state 1) is aligned with the (I) states 3 (green) and 4 (red), (J) state 5 (blue), (K) state 6 (cyan), and (L) state 7 (yellow). In (E–H), the residues at the PET-binding site are colored dark green. In (E–L), the three catalytic residues (Ser160, Asp206, and His237) are colored in orange. State 2 is structurally similar to state 1 (native structure); thus, it is not shown. Full PETase structural illustrations are shown in Figure S4.

1A), Thermo-PETase exhibits more flexibility in regions involving two catalytic residues at 298 K (Figure 1G). Upon increasing the temperature to 308 K, the D-loop in Thermo-PETase appears to be more stable than it in WT-PETase, while the flexibility of the region close to His237 in Thermo-PETase is still more pronounced than that in WT-PETase, as demonstrated by RMSF (Figure 1H) and the contact probability map (Figure S3). The W-loop, which was identified as one of the most flexible regions in WT-PETase, has negative effects on its overall thermostability.^{32,63} Mutation on the residues within the W-loop (e.g., Asp186) in order to form stable electrostatic interactions or hydrogen bonds has been demonstrated as a practice strategy for enhancing the thermostability of PETase.^{21,33} Our simulations reveal that mutations in Thermo-PETase stabilize the W-loop by reducing the structural flexibility, potentially contributing to increased stability. On the other hand, the W-loop in Thermo-PETase remains consistently more stable than it is in WT-PETase across different temperatures. This observation is reminiscent of the findings from a recent study, which has underlined the advantageous role of a rigid, correctly oriented Trp185 in stabilizing the binding interactions with the substrate.³³

To better illustrate the structural flexibility of PETase and its changes with increasing temperature, we mapped the RMSF values onto the native structures of WT- and Thermo-PETase (Figure 1I). Noteworthy, the RMSD between the PDB structures of WT- and Thermo-PETase is only 0.02 nm, indicating that these two PETases share a high degree of similarity in the static native structure. However, notable differences in structural dynamics are evident, particularly in regions close to the PET-binding site. Furthermore, at the low temperature of 298 K, the D- and W-loops in WT-PETase exhibit certain degrees of flexibility, while most regions in WT-PETase are relatively static, including the PET-binding site. As the temperature increases to 308 K, the binding site of WT-PETase becomes dynamic. The flexible binding site in PETase may potentially facilitate substrate binding, contributing to the increased PET-degradation efficiency.⁴⁰ In contrast, despite having a more rigid W-loop, Thermo-PETase at 298 K exhibits excessive structural flexibility at the binding site, which becomes even more dynamic as the temperature increases to 308 K. These distinct observations of structural dynamics between WT- and Thermo-PETase may influence substrate

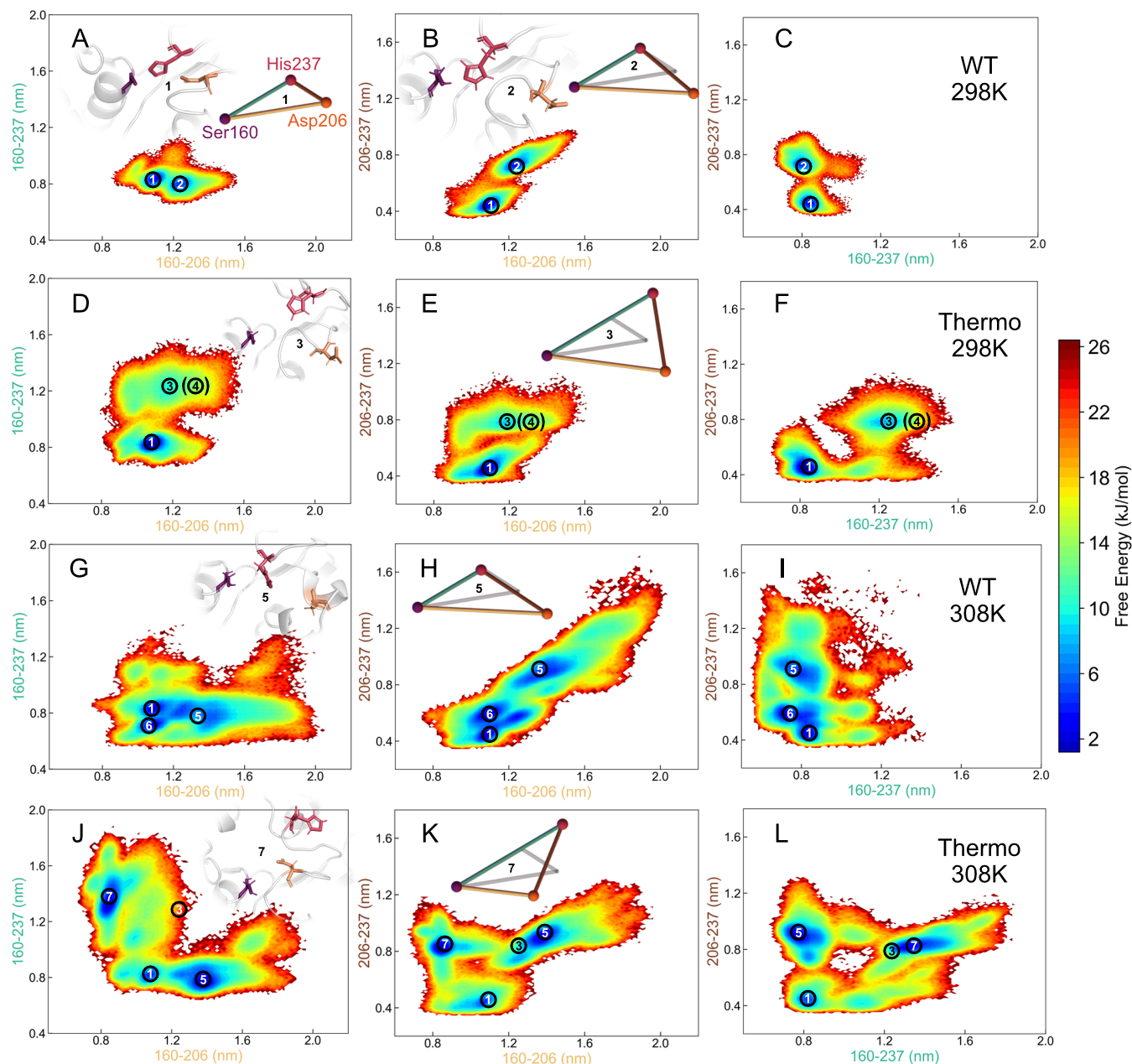


Figure 3. FELs projected onto the distances between every pair of the catalytic triad of Ser160, Asp206, and His237. FELs at 298 K for (A–C) WT-PETase and (D–F) Thermo-PETase. FELs at 308 K for (G–I) WT-PETase and (J–L) Thermo-PETase. Typical structures of PETase focusing on the catalytic triad in different (meta)stable states are shown. The (meta)stable states are numbered in the same manner as they are in Figure 2. Colored triangles depict the geometries of the catalytic sites of PETase at different (meta)stable states, while the gray triangle depicts the geometry of the catalytic site in the native structure of WT-PETase (state 1). The pairwise distances of the catalytic residues in state 6 are similar to those in state 1 (native structure), thus the structural illustration of state 6 is not shown.

binding, thus, further making distinct contributions to the catalytic activity of PETase.

FELs of PETase in the Native State. In order to capture the essential structural dynamics of PETase at the native states, we collected the simulation trajectories of WT- and Thermo-PETase at the same ambient temperatures (298 and 308 K), where both PETases remained folded, and subsequently performed PCA. At 298 K, the FELs projected onto the PC1 and PC2 reveal that WT-PETase explores a notably smaller conformational space compared to Thermo-PETase, indicating significant structural flexibility in Thermo-PETase at low temperatures (Figure 2A and B). At 308 K, although the area

of FELs is comparable for WT- and Thermo-PETase, the conformational spaces explored by these two PETases are significantly different, leading to distinct structural dynamics (Figure 2C and D).

Further projections of simulation trajectories onto the PCs with structural illustrations showcase the key motions in PETase (Figure 2E–H). We observed that the most dominant structural dynamics in these two PETases at both temperatures are related to the collective motions led by the PET-binding site and catalytic site. Specifically, at 298 K, the D-loop exhibits a twisting motion along PC1, whereas it swings in the opposite direction from the loop hosting His237 along PC2. This

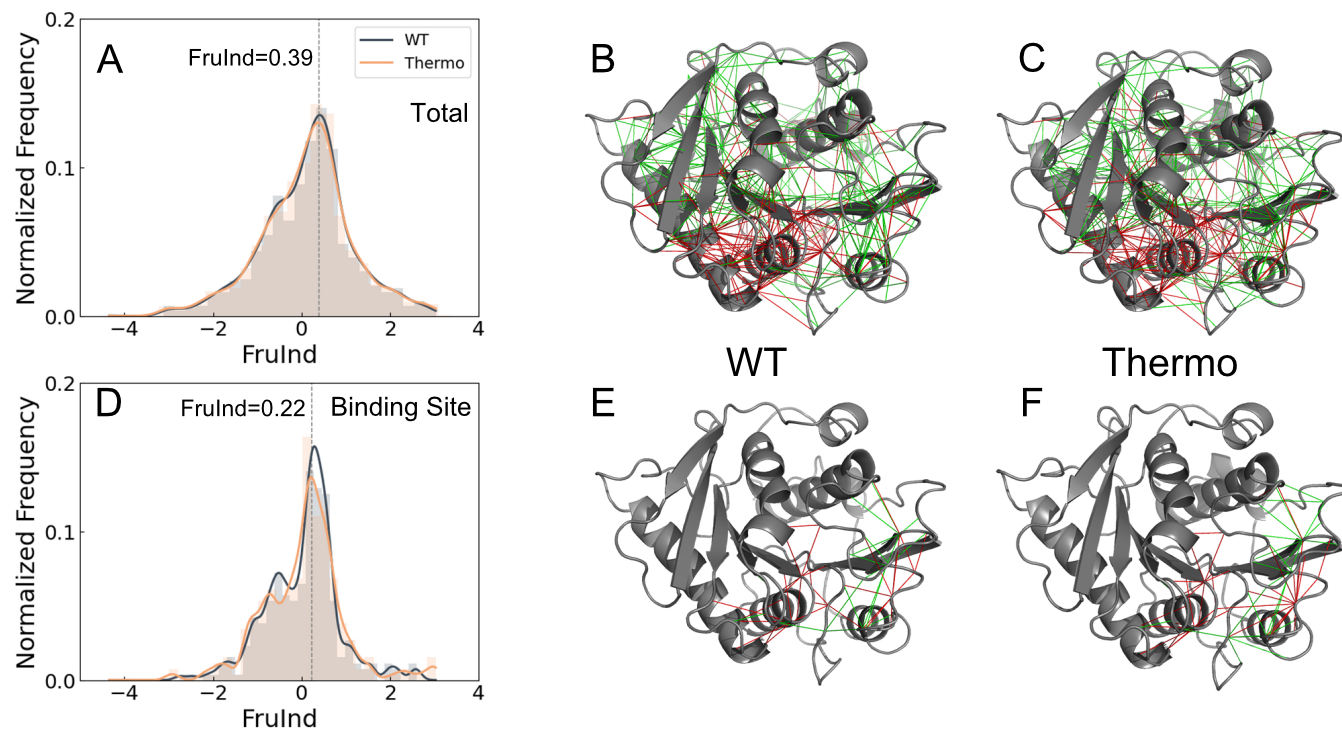


Figure 4. Local frustrations in WT- and Thermo-PETase. (A) Distribution of the *FruInd* for contacts involving all residues, with a dashed gray line indicating the most probable value. Visualization of total minimally and highly frustrated contacts on the native structures of (B) WT- and (C) Thermo-PETase, respectively. (D–F) Same as (A–C), but specifically for contacts involving residues within the binding site. In (B), (C), (E), and (F), green lines represent the minimally frustrated contacts, while red lines represent the highly frustrated contacts.

motion along PC2 may correspond to a conventional “open-to-close” conformational transition in PETase,^{38,64} potentially in favor of accommodating PET-binding. Furthermore, the FEL of WT-PETase features a single, wide basin, which includes the native state (denoted as state 1) and native-like state 2. In contrast, the FEL of Thermo-PETase displays three widely distributed energy basins, with the most probable one corresponding to the native state. Thermo-PETase within the right-most basin (denoted as state 4) and the intermediate basin (denoted as state 3) both show a more elongated D-loop (Figure 2I), which may facilitate PET binding.⁶⁵

The collective motion patterns in PETase vary significantly as the temperature changes. When the temperature increases to 308 K, the structural dynamics of PETase along PC1 and PC2 predominantly concentrate on the PET-binding site and are strongly related to the “open-to-close” transition (Figure 2G and H). In this respect, state 5, which was found to be highly populated in both WT- and Thermo-PETase, exhibits an open-binding site (Figure 2J), serving as a binding-competent state. In addition, distinct structural dynamic behaviors were observed for these two PETase, as evidenced by the more widely distributed FEL of WT- and Thermo-PETase focusing along PC2 and PC1, respectively. It is worth noting that the collective motion of PETase along PC2 involves a twisting mode, which may lead to an incomplete opening of the binding site for PET. Careful analysis on the structures of PETase in states 6 and 7 (Figure 2K and L), which are respectively populated by WT- and Thermo-PETase, reveals no clear expansion in the binding cleft; thus, their roles in PET binding remain elusive.

To elucidate the structural dynamics of PETase at the catalytic site, we projected the FELs onto the spatial distances between every pair of residues in the catalytic triad Ser160,

Asp206, and His237 (Figure 3). At 298 K (Figure 3A–F), WT-PETase explores a much narrower conformational space than that of Thermo-PETase, with two (meta)stable states observed (states 1 and 2). Noteworthy, while WT-PETase in state 2 is overall structurally similar to the native structure shown in Figure 2, it possesses a slightly opened catalytic triad, compared to that in state 1. The existence of state 2 for WT-PETase may facilitate this enzyme to bind and consequently degrade PET at room temperature.⁴⁰ On the other hand, Thermo-PETase in states 3 and 4 exhibits similarly increased pairwise distances among these three catalytic residues compared to WT-PETase. This indicates that the structural flexibility of Thermo-PETase at the catalytic site is significantly enhanced by the mutations, thus promoting the binding of PET.

At 308 K (Figure 3G–L), although WT- and Thermo-PETase display comparable overall areas of FELs, they are populated at different (meta)stable states. Apart from the shared states 1 and 5, where PETase exhibits the cleft-open, binding-competent structure, WT- and Thermo-PETase were also found to be populated at states 6 and 7, respectively. Detailed analysis reveals that WT-PETase maintains structural similarity at the catalytic site between states 1 and 6, indicating that WT-PETase in state 6 may not be advantageous for PET binding. On the other hand, Thermo-PETase in state 7 features an open-binding cleft with the elongated pairs of Ser160–His237 and Asp206–His237, thus rendering it a binding-competent state for promoting PET binding. In addition, it is evident that Thermo-PETase can explore more conformational space at large distance values of Asp206–His237. It is worth noting that the Asp206–His237 bridge serves as a critical structural scaffold for substrate accommodation and directly interacts with PET molecules (Figures

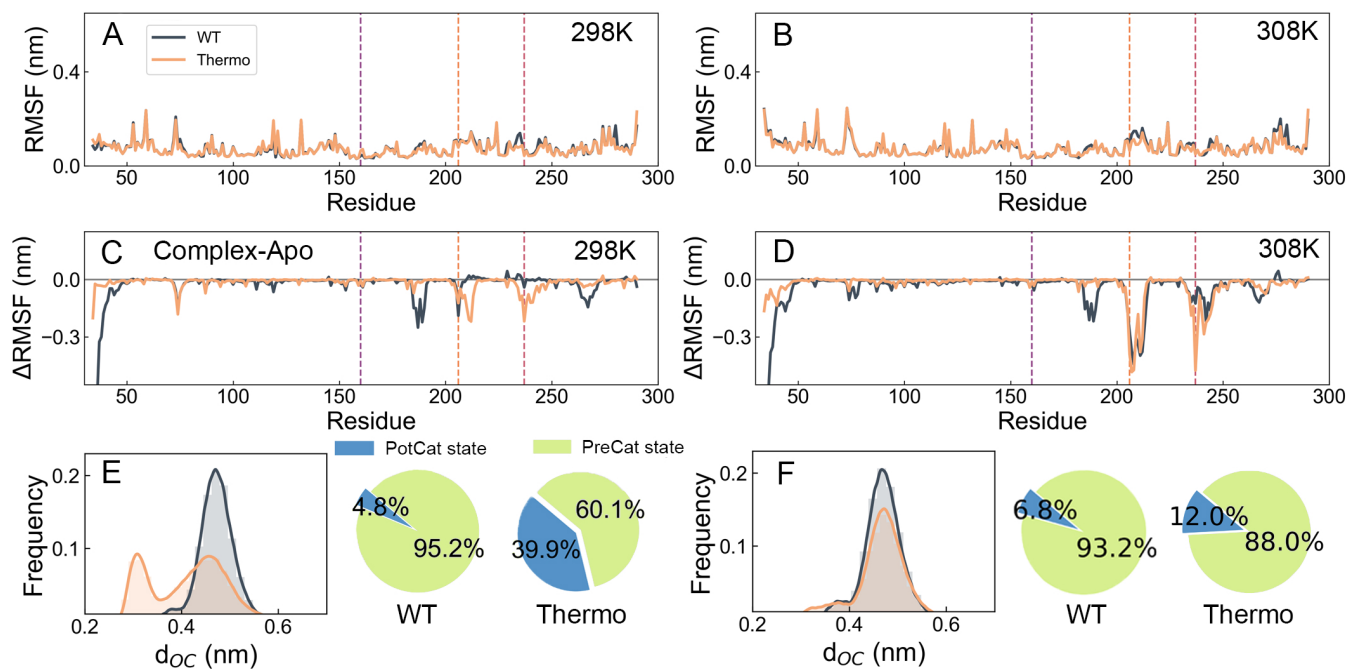


Figure 5. Structural Dynamics of PETase upon substrate binding. RMSF of WT- and Thermo-PETase binding with the substrate at (A) 298 K and (B) 308 K. RMSF differences of PETase between the apo state and the binary substrate–complex state for WT- and Thermo-PETase at (C) 298 K and (D) 308 K. Normalized frequency distribution of spatial distance d_{OC} between the oxygen O₂ and the carbonyl carbon C of the substrate and population distribution of the potentially catalytically competent (“PotCal”) state and precatalytically competent (“PreCal”) state during MD simulations performed at (E) 298 K and (F) 308 K. The “PotCal” state and “PreCal” state are defined by a threshold of d_{OC} of 0.4 nm.

II and S1). In this respect, the extended and flexible Asp206–His237 pair possessed by Thermo-PETase may assist PET binding through excessive structural fluctuations.

Frustrations in the Native Structure of PETase. A naturally evolved, well-folded protein adheres to the “principle of minimal frustration”,⁶⁶ which typically results in a funneled energy landscape. However, conflicting inter-residue interactions, known as frustrated contacts, are frequently observed in the native structures of proteins. Although these interactions generally weaken the stability of native structures, they can promote specific structural dynamics that may be related to functional purposes.⁶⁷ To assess the presence of frustrated contacts in WT- and Thermo-PETase, we quantified frustrations in the native structures of these two PETases using the method introduced by Ferreiro et al.⁶⁸ In brief, this method compares the energetic contribution to the additional stabilization provided to a pair of residues in the native structure with the statistical distribution of energies that would result from placing different residues in the same position. A native pair is deemed a highly frustrated contact if it induces significant destabilization compared with other possibilities. In other words, the native energy of a highly frustrated pair should be at the high end of the distribution. Conversely, for a minimally frustrated contact, its native energy should occupy the lower end of the energy distribution. This indicates that the minimally frustrated contact is relatively stable in the native structure, while any mutation affecting this contact will likely increase the energy, leading to structural destabilization. To measure the level of frustration, a quantity called the frustration index (*FruInd*) was introduced.⁶⁸ *FruInd* is calculated as the ratio of the additional stabilization energy for an individual native pair to the typical fluctuation in the energy distribution. Thus, a high (low) value of *FruInd* indicates a low (high) degree of frustration for the contact.

The threshold of *FruInd* for determining whether a contact is highly or minimally frustrated was taken from Ferreiro et al.⁶⁸

We observed wide distributions of *FruInd* for both WT- and Thermo-PETase, with highly frustrated contacts being only weakly populated (Figure 4A–C and Table S1). Additionally, the distributions of *FruInd* for WT- and Thermo-PETase largely overlap, suggesting that the three mutations in Thermo-PETase may not lead to significant changes in the frustrations of the native structures. These results imply that both PETase and its variant have largely eliminated the highly frustrated interactions in their native states, resulting in stable structures as robust scaffolds for function. Focusing on the PET-binding site, we observed that the distributions of *FruInd* for WT- and Thermo-PETase slightly shift to the left, indicating an accumulation of highly frustrated contacts at the binding site (Figure 4D). This suggests that the binding site of PETase is fragile and prone to deformation.⁶⁹ Furthermore, notable differences in frustration were observed between WT- and Thermo-PETase (Figure 4E and F). Detailed comparisons at the binding site reveal that Thermo-PETase exhibits lower values in the *FruInd* distribution and possesses more highly frustrated contacts than does WT-PETase. These findings together suggest that WT- and Thermo-PETase may share globally similar structural dynamics, with discrepancies primarily observed locally at the binding site, where Thermo-PETase displays more significant structural flexibility than WT-PETase.

Dynamics of PETase upon PET Binding. Structural flexibility of enzymes at catalytic sites can be advantageous for substrate recruitment and product release,^{70,71} however excessive structural dynamics at catalytic sites may induce large catalytic distances, thereby impeding chemical reactions. In order to see how PET binding impacts the structural dynamics of PETase and subsequent catalysis, we performed

molecular docking of a 4PET with PETase (Figure S1). The complex structure of PET:PETase obtained through docking is consistent with those from the previous studies,^{19,54} and subsequently was used as the initial structure for the MD simulations at ambient temperatures (298 and 308 K).

It has been proposed that the nucleophilic attack carried out by Ser160 to the carbonyl group of the benzene ring of the substrate PET molecules is essential for initializing the hydrolysis of PET polymer by PETase.^{37,58,59} In this regard, we calculated the distance (d_{OC}) between the oxygen O_γ of the catalytic Ser160 and the carbonyl carbon C of the substrate during MD simulations (Figure S6), considering that a chemical reaction occurs only when the involving atoms are spatially close. At 298 K, both WT- and Thermo-PETase keep the distance d_{OC} at relatively low values, which is optimal for the subsequent catalytic reaction. When the temperature increases to 308 K, the distance d_{OC} during the simulations largely remained at small values. We note that large fluctuations in d_{OC} were observed occasionally ($d_{OC} > 0.6$ nm) at both temperatures, leading to substrate drifting away from the binding site. Due to the inherent flexible characteristics of the polymer, the enzyme–substrate bound state was observed to be flexible in our simulations, consistent with previous studies.^{54,72} In PET, the backbone adopts two different conformations, *trans* and *gauche*, which can have different impacts on the degradation efficiency of PETase.⁶⁴ To explore the main conformation of 4PET when bound with PETase, we performed analysis on the O–C–C–O torsion angle in the ethylene glycol (EG) units of the 4PET substrate (Figure S6). We found that the *gauche* conformation comprises about 90% of the PET conformational ensembles at both 298 and 308 K, similar to previous observations for amorphous PET film.³⁹ These results further suggest that the binding modes in our study resemble the binding of a low-crystallinity PET film with PETase.

In order to assess the structural dynamics of PETase upon substrate binding, we extracted the trajectories when 4PET is bound with PETase and calculated the RMSF of PETase (Figures 5A,B and S7). Interestingly, we found that the RMSF profiles of WT- and Thermo-PETase in the PET-bound binary complexes are very similar. This is different from PETase at the apo state, where arresting discrepancies were found upon mutations (Figure 1). Detailed comparisons of RMSF profiles between WT- and Thermo-PETase indicate that Thermo-PETase has overall smaller RMSF values than WT-PETase, in particular at the catalytic residues of Asp206 and His237. Further structural analysis reveals that the catalytic triad of PETase in the bound complex is very similar for both WT- and Thermo-PETase (Figure S8), resembling that in the native structure of PETase in its apo state. Our findings indicate that WT- and Thermo-PETase share similar structures and dynamics when they are bound with the substrate.

We observed extensive quenching of structural dynamics in PETase bound with 4PET (Figure 5C and D). In detail, the most significant dynamics quenching effects for WT-PETase occurred within the W-loop. The side chain of Trp185 has been found to adopt three conformations in the native structure of WT-PETase.^{37,38} Quenching the structural dynamics of Trp185 and adapting its structure toward the one in the PET-binding state are crucial steps in realizing the catalysis of PETase, leading to the major difference between mesophilic and thermophilic PET hydrolases. On the other hand, 4PET significantly stabilizes the catalytic residues

Asp206 and His237 in Thermo-PETase, and thus, the dynamics of the catalytic triad observed in the apo state has been largely quenched. As the stable catalytic sites and spatially closed catalytic distances are prerequisites for catalysis, 4PET binding stabilizes structures of Thermo-PETase more than those of WT-PETase, possibly due to the fact that the interactions formed between substrate and enzyme are stronger and more widely distributed in Thermo-PETase than WT-PETase (Figure S9).

By analyzing the d_{OC} distribution, we found that Thermo-PETase exhibits a higher population at smaller d_{OC} values when bound with 4PET (Figure 5E and F). A smaller distance between the catalytic serine of the enzyme and the labile carbonyl of the substrate often suggests a higher probability for the hydrolytic reaction to take place.⁷³ Here, we chose 0.4 nm as the threshold for defining the state with a small d_{OC} , which is potentially competent to trigger catalysis (referred to as the “PotCat state”), and the state with too large d_{OC} to trigger catalysis (referred to as the “PreCat state”). The higher population of the “PotCat” state for Thermo-PETase than that for WT-PETase implies that Thermo-PETase may more readily trigger the subsequent catalytic reaction, potentially contributing to its enhanced efficiency. As the temperature increased from 298 to 308 K, we observed a decreasing population of the “PotCat” state for Thermo-PETase, while WT-PETase maintained similar distributions of the “PotCat” and “PreCat” states. Our results suggest that the catalytic sites of Thermo-PETase, compared with those of WT-PETase, are more sensitive to external stimuli such as substrate binding and temperature changes.

CONCLUSIONS

In this work, we used MD simulations and local frustration analysis to investigate how the three mutations (S121E, D186H, and R280A) contribute to the enhanced PET-degradation efficiency of Thermo-PETase. Experiments have demonstrated that Thermo-PETase exhibits enhanced PET-degradation activity compared to WT-PETase, even at low temperatures,^{21,25} where both PETases remain well-folded. Previous studies have revealed that, unlike thermophilic PET hydrolases, which have rigid, closed active sites and show no PET-degradation activity at moderate (mesophilic) temperatures, the active-site flexibility in PETase is crucial for efficient PET degradation.⁴⁰ Although the initial design objective for Thermo-PETase was to increase the thermostability of the enzyme by introducing additional stabilizing interactions,²¹ we observed significant enhancements in structural flexibility at the PET-binding sites. The open and dynamic nature of the active-site cleft has been recognized as a critical factor enabling PETase to function at ambient temperatures, providing a distinct catalytic advantage over thermophilic hydrolases.³⁸ Our results align with these findings, showing that Thermo-PETase has increased both global thermostability and local flexibility, potentially contributing to the overall enhancement of PET degradation observed in the experiments. The high similarity between the native structures of WT- and Thermo-PETase has resulted in a similar overall pattern of frustrated contact. However, a detailed analysis of the local regions shows distinct frustration levels between these two PETases. The introduction of the three mutations in Thermo-PETase increases the degree of frustration at the local PET-binding sites, making Thermo-PETase more prone to deformation in favor of accommodating the substrate during binding

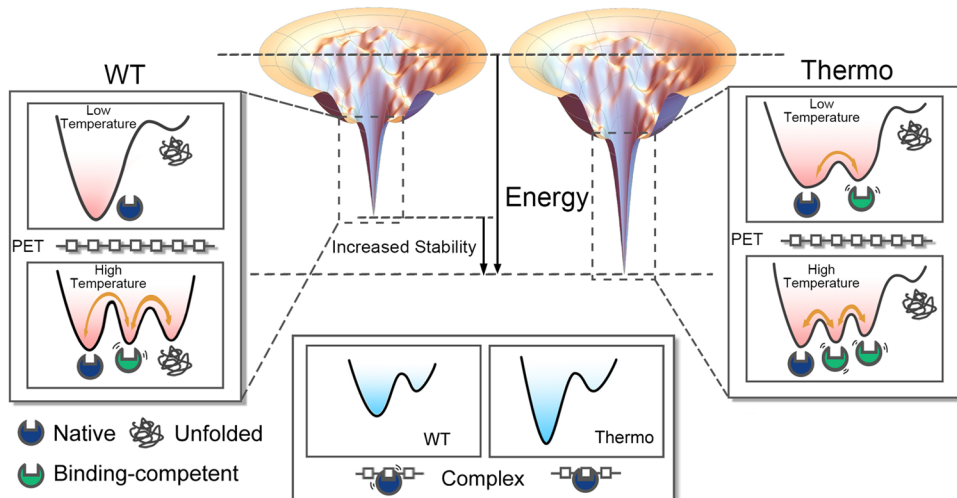


Figure 6. Energy landscapes and FELs of WT- and Thermo-PETase. The funneled energy landscapes of WT- and Thermo-PETase show arresting differences in the depth of funnels (upper center), suggesting increased stability for Thermo-PETase upon triple mutations. With close examination at the bottom of the funnel, WT- and Thermo-PETase exhibit distinct free energy profiles (left and right), each showcasing unique temperature responses. Orange arrows denote the transitions between states near the native state with arrow thickness representing the ease of these transitions. Upon PET binding (lower center), these two PETases have the same catalytically competent native structure with PET being more loosely bound with WT-PETase than Thermo-PETase.

compared to WT-PETase. Notably, our results from both MD simulations and frustration analysis on the apo form of PETase reveal the dynamic picture of PETase when recruiting the PET substrate, reminiscent of recently proposed conformational selection for the PETase:PET complex initiation.⁶⁴ Interestingly, we found that substrate binding significantly reduces the structural dynamics of Thermo-PETase induced by the mutations, resulting in a stable catalytic triad similar to that of WT-PETase. Furthermore, we observed increases in substrate–enzyme interchain contacts in Thermo-PETase, leading to more populated catalytically competent states for chemical reactions compared to WT-PETase. Collectively, we propose that the effects of mutations in Thermo-PETase on improving the PET-degradation performance may be multifaceted: (1) enhancing the overall stability of the enzyme for increasing its tolerance to environmental changes; (2) increasing the local structural flexibility at the binding site, which is advantageous for substrate recruitment and product release; and (3) quenching the structural dynamics of the enzyme at catalytic sites upon substrate binding, a prerequisite for chemical reactions.

Substrate-binding residues are important for enzymatic activity. Previous studies identified a unique conformationally dynamical equilibrium of the Trp185 side chain wobbling between conformers A, B, and C in PETase.^{37,38} This has made PETase distinguishable from other homologous enzymes such as thermophilic PET hydrolases, where the equivalent conserved Trp adopts conformer C (Figure S10). Structural analysis indicates that the substrate can only bind to PETase with Trp185 in conformer B by forming stacked interactions with one of the rings in PET molecules, while other conformers of Trp185 would clash with the substrate, thus hindering the binding.³⁷ Recent experiments and simulations have underlined the importance of the unique amino acids Ser214 and ILe218 of WT-PETase in triggering the high mobility of Trp185, thereby proposing a general mechanism for improving the catalytic activity of thermophilic PET hydrolases through the permission of the “wobbling” dynamics

of Trp185.^{63,74} Interestingly, our simulation results reveal that the conformational dynamics of Trp185 in Thermo-PETase have vanished, associated with a stabilized W-loop, compared to WT-PETase. Detailed structural analysis shows that Trp185 in Thermo-PETase is already in conformer B (Figure S10), thus facilitating the subsequent substrate binding. It is worth noting that great efforts have been made recently on mutating residues in the W-loop, aiming at fixing Trp185 in conformer B while simultaneously enhancing the overall stability.^{26,32,33} Consequently, the mutations in Thermo-PETase have effectively stabilized both the local structure at Trp185 toward the substrate-binding conformation and the global structure by introducing a hydrogen bond (S121E/D186H) at the W-loop, which is one of the most flexible regions in WT-PETase.^{21,75}

Conventionally, the practical design of WT-PETase aims to improve thermostability by reducing the structural flexibility,^{21,24–27,29,30,32,33,76} as stability and flexibility are usually considered to be coupled in proteins. For instance, the residues within the highly flexible W-loop of WT-PETase have been targeted as hot spots for engineering. Through the substitutions of Asp186 with polar or nonpolar residues in the W-loop,^{21,32,33} most PETase variants exhibited increased melting temperatures along with enhanced catalytic activity, compared to WT-PETase. From the energy landscape perspective, the stability of a protein can be determined by the funnel-like topography of its folding energy landscape.^{77,78} In this regard, mutations aiming at introducing stabilized interactions in the native state, which corresponds to the bottom of the funnel, will deepen the energy landscape, thus leading to increased thermostability (Figure 6). Interestingly, our simulations reveal that the improvements in the catalytic activity of Thermo-PETase can be partially attributed to the enhanced structural flexibility of the enzyme in its native state. In other words, in addition to increasing the depth of the funnel, mutations in Thermo-PETase have unprecedented effects on modulating the shape of the energy landscape at the bottom of the funnel. At low temperature, Thermo-PETase can explore a wider range of conformational space than WT-

PETase. Mutations enable Thermo-PETase to switch between the native structure resembling WT-PETase and the PET binding-competent structure with the open and flexible active cleft, which promotes substrate binding. This binding-competent structure can be highly populated for WT-PETase only at elevated temperatures, where Thermo-PETase becomes more flexible in rendering multiple binding-competent structures. However, WT-PETase is heat-labile and prone to denaturation, slowing down its catalytic activity at high temperatures. Upon PET binding, the extensive structural dynamics of Thermo-PETase are largely quenched by PET, leading to a stable catalytically competent native structure, the same as WT-PETase. Furthermore, we found that the complex formed by WT-PETase and PET switch between two states ("PotCat" and "PreCat" states), supported by the NMR experiments, where PET in the binding cleft of PETase was found to be highly dynamic.^{39,79} Compared to WT-PETase, Thermo-PETase, which forms more extensive contacts with PET and is dynamically quenched, exhibits closer distances for nucleophilic attack, thus leading to higher chances for PET hydrolytic reactions to take place. In conclusion, mutations in Thermo-PETase have decoupled the interplay between global stability and local flexibility of the enzyme, thus improving the catalytic performance of Thermo-PETase over WT-PETase across a wide range of temperatures.²¹

The PET-degradation process is complex, involving both the adsorption of PETase to the PET polymeric chain and the chemical reaction that breaks down the PET polymer into its constituting monomers. Unlike thermophilic PET-degrading enzymes, PETase can depolymerize PET at moderate temperatures.¹⁸ This unique functionality of PETase is largely due to its structural characteristics, particularly its open active-site cleft, which provides high accessibility for substrate binding,³⁸ thereby enhancing PET-degradation activity at moderate temperatures. In this study, we focused on characterizing the structural dynamics of PETase and its variant, aiming to elucidate the roles of mutations in Thermo-PETase in facilitating substrate binding and stabilizing the initial PETase:PET complex. However, our study, which does not explore the chemical reaction, has limitations in fully understanding the PET-degradation process. Recently, García-Meseguer et al. used hybrid quantum mechanics/molecular mechanics (QM/MM) MD simulations to characterize the catalytic mechanisms of FAST-PETase compared to WT-PETase.⁵⁸ They found that although all five mutations in FAST-PETase are far from the active site, they play important roles in stabilizing the transition state by indirectly impacting the catalytic triad, leading to lowering of the free energy barriers during the chemical reaction. This study, along with our work, suggests that the mutations in Thermo- and FAST-PETase, initially designed to improve thermostability, may also enhance substrate binding and catalysis, ultimately accelerating PET depolymerization.

In summary, our results reveal that the stability and flexibility of enzymes are not necessarily correlated, in contradiction to the convention that high (low) stability usually leads to a rigid (flexible) protein structure.⁸⁰ It is worth noting that recent work has observed a decoupling interplay between the stability and flexibility in a computationally designed hydrolase Turbo-PETase, which has demonstrated superior performance compared to other PET hydrolases to date.³⁰ The high PET depolymerization efficiency of Turbo-PETase was attributed to the mutations that have resulted in

both increases in thermostability at the global scale and structural flexibility at the PET-binding site, exhibiting elevated melting temperature and simultaneously enabling the promiscuous attack to different PET surface structures.³⁰ This significant achievement made by Turbo-PETase has paved a promising way for future PETase design, focusing on enhancing both thermostability and flexibility. Recently, AI-aided protein design has become increasingly popular and efficient, particularly for structural design and functional optimization.⁸¹ Various deep-learning protein sequence engineering methods can be applied to create enzymes with enhanced catalytic efficiency.^{82–84} A notable success in this field is FAST-PETase, which exhibits significantly improved catalytic activity over a wide range of temperatures compared to WT-PETase and Thermo-PETase.²⁵ FAST-PETase utilizes deep learning techniques to predict optimal amino acids in the local structural environments of WT-PETase, based on training with over 19,000 protein structures from the PDB. Our study shows that both global stability and local flexibility of PETase are crucial for achieving highly efficient PET-degradation activity. This underscores the necessity for AI tools to manage the delicate balance between stability and flexibility in PETase design, with the goal of optimizing PET degradation at ambient temperatures. Although a full mechanistic understanding of achieving optimal stability–flexibility balance in PETase for maximizing PET-degradation efficiency remains elusive, our findings suggest that future mutations aimed at enhancing PETase enzymatic activity should carefully consider the trade-off between stability and flexibility. Our study offers valuable insights into the rational design strategy to improve the PET-degradation performance of PETase, where both the structure and dynamics of the enzyme should be simultaneously considered.

ASSOCIATED CONTENT

Data Availability Statement

The necessary files for setting up Gromacs simulations and molecular docking, as well as the frustration analysis results are publicly available at <https://osf.io/9yzjf/>. Additional data can be found in Supporting Information.

Supporting Information

The Supporting Information is available free of charge at <https://pubs.acs.org/doi/10.1021/acs.jcim.4c00877>.

Details about the frustration analysis are organized in a table; graphs illustrating structures in greater detail, additional MD simulation trajectories, contact maps, and distributions of pairwise distances for the three residues of the catalytic triad in WT- and Thermo-PETase at different temperatures, with and without substrate binding ([PDF](#))

AUTHOR INFORMATION

Corresponding Author

Xiaokun Chu – Advanced Materials Thrust, Function Hub, The Hong Kong University of Science and Technology (Guangzhou), Guangzhou, Guangdong 511400, China; Guangzhou Municipal Key Laboratory of Materials Informatics, The Hong Kong University of Science and Technology (Guangzhou), Guangzhou, Guangdong 511400, China; Division of Life Science, The Hong Kong University of Science and Technology, Hong Kong SAR 999077, China;

orcid.org/0000-0003-3166-7070; Email: xiakunchu@hkust-gz.edu.cn

Authors

Shiqinrui Xu — Advanced Materials Thrust, Function Hub,
The Hong Kong University of Science and Technology
(Guangzhou), Guangzhou, Guangdong 511400, China;
orcid.org/0009-0000-5480-546X

Chengze Huo — Advanced Materials Thrust, Function Hub,
The Hong Kong University of Science and Technology
(Guangzhou), Guangzhou, Guangdong 511400, China;
orcid.org/0009-0005-9550-7123

Complete contact information is available at:
<https://pubs.acs.org/10.1021/acs.jcim.4c00877>

Notes

The authors declare no competing financial interest.

ACKNOWLEDGMENTS

The project was supported by the National Key R&D Program of China (No. 2023YFC3905000) and the Guangdong Scientific Research Platform and Projects for Higher-educational Institutions from the Department of Education of Guangdong Province (Grant No. 2023KTSCX169). X.C. was also partly supported by the Municipal Key Laboratory Construction program of the Guangzhou Municipal Science and Technology Project (Grant No. 2023A03J0003). The authors acknowledge the Green e Materials (GeM) Laboratory and HPC+AI Intelligence Computing Center at the Hong Kong University of Science and Technology (Guangzhou) for providing computational support.

REFERENCES

- (1) Moharir, R. V.; Kumar, S. Challenges Associated with Plastic Waste Disposal and Allied Microbial Routes for Its Effective Degradation: A Comprehensive Review. *J. Cleaner Prod.* **2019**, *208*, 65–76.
- (2) Awoyera, P. O.; Adesina, A. Plastic Wastes to Construction Products: Status, Limitations and Future Perspective. *Case Stud. Constr. Mater.* **2020**, *12*, e00330.
- (3) Ali, S. S.; Elsafty, T.; Koutra, E.; Kornaros, M.; El-Sheekh, M.; Abdelkarim, E. A.; Zhu, D.; Sun, J. Degradation of Conventional Plastic Wastes in the Environment: A Review on Current Status of Knowledge and Future Perspectives of Disposal. *Sci. Total Environ.* **2021**, *771*, 144719.
- (4) Jambeck, J. R.; Geyer, R.; Wilcox, C.; Siegler, T. R.; Perryman, M.; Andrady, A.; Narayan, R.; Law, K. L. Plastic waste inputs from land into the ocean. *Science* **2015**, *347*, 768–771.
- (5) Geyer, R.; Jambeck, J. R.; Law, K. L. Production, use, and fate of all plastics ever made. *Sci. Adv.* **2017**, *3*, e1700782.
- (6) Sinha, V.; Patel, M. R.; Patel, J. V. PET waste management by chemical recycling: a review. *J. Polym. Environ.* **2010**, *18*, 8–25.
- (7) Law, K. L.; Starr, N.; Siegler, T. R.; Jambeck, J. R.; Mallos, N. J.; Leonard, G. H. The United States' Contribution of Plastic Waste to Land and Ocean. *Sci. Adv.* **2020**, *6*, eabd0288.
- (8) Wei, R.; Zimmermann, W. Biocatalysis as a green route for recycling the recalcitrant plastic polyethylene terephthalate. *Microb. Biotechnol.* **2017**, *10*, 1302.
- (9) Papadopoulou, A.; Hecht, K.; Buller, R. Enzymatic PET degradation. *Chimia* **2019**, *73*, 743.
- (10) Taniguchi, I.; Yoshida, S.; Hiraga, K.; Miyamoto, K.; Kimura, Y.; Oda, K. Biodegradation of PET: current status and application aspects. *ACS Catal.* **2019**, *9*, 4089–4105.
- (11) Kawai, F.; Kawabata, T.; Oda, M. Current knowledge on enzymatic PET degradation and its possible application to waste stream management and other fields. *Appl. Microbiol. Biotechnol.* **2019**, *103*, 4253–4268.
- (12) Wei, Y.; Swenson, L.; Castro, C.; Derewenda, U.; Minor, W.; Arai, H.; Aoki, J.; Inoue, K.; Servin-Gonzalez, L.; Derewenda, Z. S. Structure of a microbial homologue of mammalian platelet-activating factor acetylhydrolases: *Streptomyces exfoliatus* lipase at 1.9 Å resolution. *Structure* **1998**, *6*, 511–519.
- (13) Müller, R.; Schrader, H.; Profe, J.; Dresler, K.; Deckwer, W.-D. Enzymatic Degradation of Poly(Ethylene Terephthalate): Rapid Hydrolyse Using a Hydrolase from *T. Fusca*. *Macromol. Rapid Commun.* **2005**, *26*, 1400–1405.
- (14) Ronkvist, Å. M.; Xie, W.; Lu, W.; Gross, R. A. Cutinase-catalyzed hydrolysis of poly (ethylene terephthalate). *Macromolecules* **2009**, *42*, 5128–5138.
- (15) Sulaiman, S.; Yamato, S.; Kanaya, E.; Kim, J.-J.; Koga, Y.; Takano, K.; Kanaya, S. Isolation of a novel cutinase homolog with polyethylene terephthalate-degrading activity from leaf-branch compost by using a metagenomic approach. *Appl. Environ. Microbiol.* **2012**, *78*, 1556–1562.
- (16) Wei, R.; Breite, D.; Song, C.; Gräsing, D.; Ploss, T.; Hille, P.; Schwerdtfeger, R.; Matysik, J.; Schulze, A.; Zimmermann, W. Biocatalytic degradation efficiency of postconsumer polyethylene terephthalate packaging determined by their polymer microstructures. *Adv. Sci.* **2019**, *6*, 1900491.
- (17) Tournier, V.; Topham, C. M.; Gilles, A.; et al. An engineered PET depolymerase to break down and recycle plastic bottles. *Nature* **2020**, *580*, 216–219.
- (18) Yoshida, S.; Hiraga, K.; Takehana, T.; Taniguchi, I.; Yamaji, H.; Maeda, Y.; Toyohara, K.; Miyamoto, K.; Kimura, Y.; Oda, K. A Bacterium That Degrades and Assimilates Poly(Ethylene Terephthalate). *Science* **2016**, *351*, 1196–1199.
- (19) Joo, S.; Cho, I. J.; Seo, H.; Son, H. F.; Sagong, H.-Y.; Shin, T. J.; Choi, S. Y.; Lee, S. Y.; Kim, K.-J. Structural Insight into Molecular Mechanism of Poly(Ethylene Terephthalate) Degradation. *Nat. Commun.* **2018**, *9*, No. 382.
- (20) Erickson, E.; Shakespeare, T. J.; Bratti, F.; Buss, B. L.; Graham, R.; Hawkins, M. A.; König, G.; Michener, W. E.; Miscall, J.; Ramirez, K. J.; Rorrer, N. A.; Zahn, M.; Pickford, A. R.; McGeehan, J. E.; Beckham, G. T. Comparative performance of PETase as a function of reaction conditions, substrate properties, and product accumulation. *ChemSusChem* **2022**, *15*, e202101932.
- (21) Son, H. F.; Cho, I. J.; Joo, S.; Seo, H.; Sagong, H.-Y.; Choi, S. Y.; Lee, S. Y.; Kim, K.-J. Rational Protein Engineering of Thermo-Stable PETase from *Ideonella Sakaiensis* for Highly Efficient PET Degradation. *ACS Catal.* **2019**, *9*, 3519–3526.
- (22) Meng, X.; Yang, L.; Liu, H.; Li, Q.; Xu, G.; Zhang, Y.; Guan, F.; Zhang, Y.; Zhang, W.; Wu, J. T. Ningfeng Protein engineering of stable IsPETase for PET plastic degradation by Premuse. *Int. J. Biol. Macromol.* **2021**, *180*, 667–676.
- (23) Liu, Y.; Liu, Z.; Guo, Z.; Yan, T.; Jin, C.; Wu, J. Enhancement of the Degradation Capacity of IsPETase for PET Plastic Degradation by Protein Engineering. *Sci. Total Environ.* **2022**, *834*, 154947.
- (24) Cui, Y.; Chen, Y.; Liu, X.; et al. Computational Redesign of a PETase for Plastic Biodegradation under Ambient Condition by the GRAPE Strategy. *ACS Catal.* **2021**, *11*, 1340–1350.
- (25) Lu, H.; Diaz, D. J.; Czarnecki, N. J.; Zhu, C.; Kim, W.; Shroff, R.; Acosta, D. J.; Alexander, B. R.; Cole, H. O.; Zhang, Y.; Lynd, N. A.; Ellington, A. D.; Alper, H. S. Machine Learning-Aided Engineering of Hydrolases for PET Depolymerization. *Nature* **2022**, *604*, 662–667.
- (26) Bell, E. L.; Smithson, R.; Kilbride, S.; Foster, J.; Hardy, F. J.; Ramachandran, S.; Tedstone, A. A.; Haigh, S. J.; Garforth, A. A.; Day, P. J. R.; Levy, C.; Shaver, M. P.; Green, A. P. Directed evolution of an efficient and thermostable PET depolymerase. *Nat. Catal.* **2022**, *5*, 673–681.
- (27) Brott, S.; Pfaff, L.; Schuricht, J.; Schwarz, J.-N.; Böttcher, D.; Badenhorst, C. P.; Wei, R.; Bornscheuer, U. T. Engineering and evaluation of thermostable IsPETase variants for PET degradation. *Eng. Life Sci.* **2022**, *22*, 192–203.

- (28) Lee, S. H.; Seo, H.; Hong, H.; Park, J.; Ki, D.; Kim, M.; Kim, H.-J.; Kim, K.-J. Three-directional engineering of IsPETase with enhanced protein yield, activity, and durability. *J. Hazard. Mater.* **2023**, *459*, 132297.
- (29) Shi, L.; Liu, P.; Tan, Z.; Zhao, W.; Gao, J.; Gu, Q.; Ma, H.; Liu, H.; Zhu, L. Complete depolymerization of PET wastes by an evolved PET hydrolase from directed evolution. *Angew. Chem., Int. Ed.* **2023**, *62*, e202218390.
- (30) Cui, Y.; Chen, Y.; Sun, J.; Zhu, T.; Pang, H.; Li, C.; Geng, W.-C.; Wu, B. Computational Redesign of a Hydrolase for Nearly Complete PET Depolymerization at Industrially Relevant High-Solids Loading. *Nat. Commun.* **2024**, *15*, No. 1417.
- (31) Joho, Y.; Royan, S.; Caputo, A.; Newton, S.; Peat, T.; Newman, J.; Jackson, C.; Ardevol, A. Enhancing PET Degrading Enzymes: A Combinatory Approach. *ChemBioChem* **2024**, *25*, e202400084.
- (32) Yin, Q.; You, S.; Zhang, J.; Qi, W.; Su, R. Enhancement of the polyethylene terephthalate and mono-(2-hydroxyethyl) terephthalate degradation activity of *Ideonella sakaiensis* PETase by an electrostatic interaction-based strategy. *Bioresour. Technol.* **2022**, *364*, 128026.
- (33) Yin, Q.; Zhang, J.; Ma, S.; Gu, T.; Wang, M.; You, S.; Ye, S.; Su, R.; Wang, Y.; Qi, W. Efficient polyethylene terephthalate biodegradation by an engineered *Ideonella sakaiensis* PETase with a fixed substrate-binding W156 residue. *Green Chem.* **2024**, *26*, 2560–2570.
- (34) Wei, R.; von Haugwitz, G.; Pfaff, L.; Mican, J.; Badenhorst, C. P. S.; Liu, W.; Weber, G.; Austin, H. P.; Bednar, D.; Damborsky, J.; Bornscheuer, U. T. Mechanism-based design of efficient PET hydrolases. *ACS Catal.* **2022**, *12*, 3382–3396.
- (35) Amalia, L.; Chang, C.-Y.; Wang, S. S.; Yeh, Y.-C.; Tsai, S.-L. Recent advances in the biological depolymerization and upcycling of polyethylene terephthalate. *Curr. Opin. Biotechnol.* **2024**, *85*, 103053.
- (36) Shi, L.; Zhu, L. Recent Advances and Challenges in Enzymatic Depolymerization and Recycling of PET Wastes. *ChemBioChem* **2024**, *25*, e202300578.
- (37) Han, X.; Liu, W.; Huang, J.-W.; Ma, J.; Zheng, Y.; Ko, T.-P.; Xu, L.; Cheng, Y.-S.; Chen, C.-C.; Guo, R.-T. Structural insight into catalytic mechanism of PET hydrolase. *Nat. Commun.* **2017**, *8*, No. 2106.
- (38) Austin, H. P.; Allen, M. D.; Donohoe, B. S.; et al. Characterization and engineering of a plastic-degrading aromatic polyesterase. *Proc. Natl. Acad. Sci. U.S.A.* **2018**, *115*, E4350–E4357.
- (39) Wei, R.; Song, C.; Gräsing, D.; Schneider, T.; Bielejtsky, P.; Böttcher, D.; Matysik, J.; Bornscheuer, U. T.; Zimmermann, W. Conformational fitting of a flexible oligomeric substrate does not explain the enzymatic PET degradation. *Nat. Commun.* **2019**, *10*, No. 5581.
- (40) Fecker, T.; Galaz-Davison, P.; Engelberger, F.; Narui, Y.; Sotomayor, M.; Parra, L. P.; Ramírez-Sarmiento, C. A. Active Site Flexibility as a Hallmark for Efficient PET Degradation by *I. Sakaiensis* PETase. *Biophys. J.* **2018**, *114*, 1302–1312.
- (41) Silva, C.; Da, S.; Silva, N.; Matamá, T.; Araújo, R.; Martins, M.; Chen, S.; Chen, J.; Wu, J.; Casal, M.; Cavaco-Paulo, A. Engineered Thermobifida fusca cutinase with increased activity on polyester substrates. *Biotechnol. J.* **2011**, *6*, 1230–1239.
- (42) Araújo, R.; Silva, C.; O'Neill, A.; Micaelo, N.; Guebitz, G.; Soares, C. M.; Casal, M.; Cavaco-Paulo, A. Tailoring cutinase activity towards polyethylene terephthalate and polyamide 6, 6 fibers. *J. Biotechnol.* **2007**, *128*, 849–857.
- (43) Kan, Y.; He, L.; Luo, Y.; Bao, R. IsPETase is a novel biocatalyst for poly (ethylene terephthalate)(PET) hydrolysis. *ChemBioChem* **2021**, *22*, 1706–1716.
- (44) Berselli, A.; Ramos, M. J.; Menziani, M. C. Novel Pet-Degrading Enzymes: Structure-Function from a Computational Perspective. *ChemBioChem* **2021**, *22*, 2032–2050.
- (45) Abraham, M. J.; Murtola, T.; Schulz, R.; Páll, S.; Smith, J. C.; Hess, B.; Lindahl, E. GROMACS: High Performance Molecular Simulations through Multi-Level Parallelism from Laptops to Supercomputers. *SoftwareX* **2015**, *1*–*2*, 19–25.
- (46) Maier, J. A.; Martinez, C.; Kasavajhala, K.; Wickstrom, L.; Hauser, K. E.; Simmerling, C. ff14SB: Improving the Accuracy of Protein Side Chain and Backbone Parameters from ff99SB. *J. Chem. Theory Comput.* **2015**, *11*, 3696–3713.
- (47) Parrinello, M.; Rahman, A. Polymorphic Transitions in Single Crystals: A New Molecular Dynamics Method. *J. Appl. Phys.* **1981**, *52*, 7182–7190.
- (48) Hess, B.; Bekker, H.; Berendsen, H. J. C.; Fraaije, J. G. E. M. LINCS: A Linear Constraint Solver for Molecular Simulations. *J. Comput. Chem.* **1997**, *18*, 1463–1472.
- (49) Darden, T.; York, D.; Pedersen, L. Particle Mesh Ewald: An N-log(N) Method for Ewald Sums in Large Systems. *J. Chem. Phys.* **1993**, *98*, 10089–10092.
- (50) Morris, G. M.; Huey, R.; Lindstrom, W.; Sanner, M. F.; Belew, R. K.; Goodsell, D. S.; Olson, A. J. AutoDock4 and AutoDockTools4: Automated Docking with Selective Receptor Flexibility. *J. Comput. Chem.* **2009**, *30*, 2785–2791.
- (51) Jerves, C.; Neves, R. P.; Ramos, M. J.; da Silva, S.; Fernandes, P. A. Reaction mechanism of the PET degrading enzyme PETase studied with DFT/MM molecular dynamics simulations. *ACS Catal.* **2021**, *11*, 11626–11638.
- (52) Hanwell, M. D.; Curtis, D. E.; Lonie, D. C.; Vandermeersch, T.; Zurek, E.; Hutchison, G. R. Avogadro: an advanced semantic chemical editor, visualization, and analysis platform. *J. Cheminf.* **2012**, *4*, No. 17.
- (53) Eberhardt, J.; Santos-Martins, D.; Tillack, A. F.; Forli, S. AutoDock Vina 1.2.0: New Docking Methods, Expanded Force Field, and Python Bindings. *J. Chem. Inf. Model.* **2021**, *61*, 3891–3898.
- (54) da Costa, C. H. S.; Dos Santos, A. M.; Alves, C. N.; Martí, S.; Moliner, V.; Santana, K.; Lameira, J. Assessment of the PETase conformational changes induced by poly (ethylene terephthalate) binding. *Proteins: Struct., Funct., Bioinf.* **2021**, *89*, 1340–1352.
- (55) Wang, J.; Wolf, R. M.; Caldwell, J. W.; Kollman, P. A.; Case, D. A. Development and Testing of a General Amber Force Field. *J. Comput. Chem.* **2004**, *25*, 1157–1174.
- (56) Sousa da Silva, A. W.; Vranken, W. F. ACPYPE - AnteChamber PYthon Parser interfacE. *BMC Res. Notes* **2012**, *5*, No. 367.
- (57) Schrodinger, LLC. *The PyMOL Molecular Graphics System*, Version 1.8, 2015, <http://www.pymol.org/pymol>.
- (58) García-Meseguer, R.; Ortí, E.; Tuñón, I.; Ruiz-Pernía, J. J.; Aragó, J. Insights into the Enhancement of the Poly (ethylene terephthalate) Degradation by FAST-PETase from Computational Modeling. *J. Am. Chem. Soc.* **2023**, *145*, 19243–19255.
- (59) Burgin, T.; Pollard, B. C.; Knott, B. C.; Mayes, H. B.; Crowley, M. F.; McGeehan, J. E.; Beckham, G. T.; Woodcock, H. L. The reaction mechanism of the *Ideonella sakaiensis* PETase enzyme. *Commun. Chem.* **2024**, *7*, No. 65.
- (60) Gowers, R. J.; Linke, M.; Barnoud, J.; Reddy, T. J. E.; Melo, M. N.; Seyler, S. L.; Domański, J.; Dotson, D. L.; Buchoux, S.; Kenney, I. M.; Beckstein, O. MDAnalysis: A Python Package for the Rapid Analysis of Molecular Dynamics Simulations. In *Proceedings of the 15th Python in Science Conference* 2016; pp 98–105.
- (61) Cheng, X.; Ivanov, I.; Wang, H.; Sine, S. M.; McCammon, J. A. Nanosecond-timescale conformational dynamics of the human $\alpha 7$ nicotinic acetylcholine receptor. *Biophys. J.* **2007**, *93*, 2622–2634.
- (62) Parra, R. G.; Schafer, N. P.; Radusky, L. G.; Tsai, M.-Y.; Guzovsky, A. B.; Wolynes, P. G.; Ferreiro, D. U. Protein Frustratometer 2: A Tool to Localize Energetic Frustration in Protein Molecules, Now with Electrostatics. *Nucleic Acids Res.* **2016**, *44*, W356–W360.
- (63) Chen, C.-C.; Han, X.; Li, X.; et al. General features to enhance enzymatic activity of poly (ethylene terephthalate) hydrolysis. *Nat. Catal.* **2021**, *4*, 425–430.
- (64) Guo, B.; Vanga, S. R.; Lopez-Lorenzo, X.; Saenz-Mendez, P.; Ericsson, S. R.; Fang, Y.; Ye, X.; Schriever, K.; Bäckström, E.; Biundo, A.; Zubarev, R. A.; Furó, I.; Hakkarainen, M.; Syréen, P.-O. Conformational selection in biocatalytic plastic degradation by PETase. *ACS Catal.* **2022**, *12*, 3397–3409.

- (65) Ferreiro, D. U.; Komives, E. A.; Wolynes, P. G. Frustration, Function and Folding. *Curr. Opin. Struct. Biol.* **2018**, *48*, 68–73.
- (66) Bryngelson, J. D.; Wolynes, P. G. Spin glasses and the statistical mechanics of protein folding. *Proc. Natl. Acad. Sci. U.S.A.* **1987**, *84*, 7524–7528.
- (67) Ferreiro, D. U.; Komives, E. A.; Wolynes, P. G. Frustration in biomolecules. *Q. Rev. Biophys.* **2014**, *47*, 285–363.
- (68) Ferreiro, D. U.; Hegler, J. A.; Komives, E. A.; Wolynes, P. G. Localizing Frustration in Native Proteins and Protein Assemblies. *Proc. Natl. Acad. Sci. U.S.A.* **2007**, *104*, 19819–19824.
- (69) Chen, M.; Chen, X.; Schafer, N. P.; Clementi, C.; Komives, E. A.; Ferreiro, D. U.; Wolynes, P. G. Surveying biomolecular frustration at atomic resolution. *Nat. Commun.* **2020**, *11*, No. 5944.
- (70) Hammes, G. G. Multiple conformational changes in enzyme catalysis. *Biochemistry* **2002**, *41*, 8221–8228.
- (71) Hammes-Schiffer, S.; Benkovic, S. J. Relating protein motion to catalysis. *Annu. Rev. Biochem.* **2006**, *75*, 519–541.
- (72) Chen, L.; Fan, F.; Yang, M.; Wang, L.; Bai, Y.; Qiu, S.; Lyu, C.; Huang, J. Atomistic insight into the binding mode and self-regulation mechanism of Is PETase towards PET substrates with different polymerization degrees. *Phys. Chem. Chem. Phys.* **2023**, *25*, 18332–18345.
- (73) Baker, P. J.; Montclare, J. K. Biotransformations Using Cutinase. In *Green Polymer Chemistry: Biocatalysis and Biomaterials*; American Chemical Society, 2010; Chapter 11; pp 141–158.
- (74) Crnjar, A.; Grinén, A.; Kamerlin, S. C. L.; Ramírez-Sarmiento, C. A. Conformational Selection of a Tryptophan Side Chain Drives the Generalized Increase in Activity of PET Hydrolases through a Ser/Ile Double Mutation. *ACS Org. Inorg. Au* **2023**, *3*, 109–119.
- (75) Qu, Z.; Zhang, L.; Sun, Y. Molecular Insights into the Enhanced Activity and/or Thermostability of PET Hydrolase by D186 Mutations. *Molecules* **2024**, *29*, 1338.
- (76) Son, H. F.; Joo, S.; Seo, H.; Sagong, H.-Y.; Lee, S. H.; Hong, H.; Kim, K.-J. Structural bioinformatics-based protein engineering of thermo-stable PETase from *Ideonella sakaiensis*. *Enzyme Microb. Technol.* **2020**, *141*, 109656.
- (77) Wang, J.; Oliveira, R. J.; Chu, X.; Whitford, P. C.; Chahine, J.; Han, W.; Wang, E.; Onuchic, J. N.; Leite, V. B. Topography of funneled landscapes determines the thermodynamics and kinetics of protein folding. *Proc. Natl. Acad. Sci. U.S.A.* **2012**, *109*, 15763–15768.
- (78) Chu, X.; Gan, L.; Wang, E.; Wang, J. Quantifying the topography of the intrinsic energy landscape of flexible biomolecular recognition. *Proc. Natl. Acad. Sci. U.S.A.* **2013**, *110*, E2342–E2351.
- (79) Falkenstein, P.; Wei, R.; Matysik, J.; Song, C. *Methods Enzymology*; Elsevier, 2021; Vol. 648, pp 231–252.
- (80) Kamerzell, T. J.; Middaugh, C. R. The complex interrelationships between protein flexibility and stability. *J. Pharm. Sci.* **2008**, *97*, 3494–3517.
- (81) Ming, Y.; Wang, W.; Yin, R.; Zeng, M.; Tang, L.; Tang, S.; Li, M. A Review of Enzyme Design in Catalytic Stability by Artificial Intelligence. *Briefings Bioinf.* **2023**, *24*, bbad065.
- (82) Dauparas, J.; Anishchenko, I.; Bennett, N.; et al. Robust deep learning-based protein sequence design using ProteinMPNN. *Science* **2022**, *378*, 49–56.
- (83) Watson, J. L.; Juergens, D.; Bennett, N. R.; et al. De novo design of protein structure and function with RFdiffusion. *Nature* **2023**, *620*, 1089–1100.
- (84) Mu, J.; Li, Z.; Zhang, B.; Zhang, Q.; Iqbal, J.; Wadood, A.; Wei, T.; Feng, Y.; Chen, H.-F. Graphomer supervised de novo protein design method and function validation. *Brief. Bioinform.* **2024**, *25*, bbae135.